Journal of Bioenergetics and Biomembranes (2023) 55:249–266
https://doi.org/10.1007/s10863-023-09973-8

RESEARCH

Spatio temporal interdependent calcium and buffer dynamics regulating DAG in a hepatocyte cell due to obesity

Vedika Mishra[1] · **Neeru Adlakha**[1]

Received: 14 May 2023 / Accepted: 23 June 2023 / Published online: 18 July 2023

Abstract

Calcium ions (Ca^{2+}) serve as a crucial signaling mechanism in almost all cells. The buffers are proteins that bind free Ca^{2+} to reduce the cell's Ca^{2+} concentration. The most studies reported in the past on calcium signaling in various cells have considered the buffer concentration as constant in the cell. However, buffers also diffuse and their concentration varies dynamically in the cells. Almost no work has been reported on interdependent calcium and buffer dynamics in the cells. In the present study, a model is proposed for inter-dependent spatio-temporal dynamics of calcium and buffer by coupling reaction–diffusion equations of Ca^{2+} and buffer in a hepatocyte cell. Boundary and initial conditions are framed based on the physiological state of the cell. The effect of various parameters viz. inositol 1,4,5-triphosphate receptor (IP3R), diffusion coefficient, SERCA pump and ryanodine receptor (RyR) on spatio-temporal dynamics of calcium and buffer regulating diacylglycerol (DAG) in a normal and obese hepatocyte cell has been studied using finite element simulation. From the results, it is concluded that the dynamics of calcium and buffer impact each other significantly along the spatio-temporal dimensions, thereby affecting the regulation of all the processes including DAG in a hepatocyte cell. The proposed model is more realistic than the existing ones, as the interdependent system dynamics of calcium and buffer have different regulatory impacts as compared to the individual and independent dynamics of these signaling processes in a hepatocyte cell.

Keywords Calcium · Buffer · Finite element method · Reaction–diffusion equation · Obesity

Mathematics Subject Classification (2020) 35–04 · 65D05 · 92B05 · 65F05 · 92B05 · 65K05 · 65K10 · 65M60

Introduction

Many normal and pathological processes involve calcium ions. Elevations in cytoplasmic Ca^{2+} regulate a wide range of biological activities, including rapid processes, such as muscle contraction and neurosecretion as well as slower and more intricate ones like cell division, differentiation and apoptosis. IP_3, a second messenger produced by phospholipase C, most frequently causes the intracellular release of Ca^{2+}, whereas the stimulation of plasma membrane store-operated channels cause Ca^{2+} to enter cells (Dupont et al. 2011). There is a need for an universal Ca^{2+} homeostasis system because calcium ions are essential not only for many cellular processes along the cell's life cycle but they are also toxic to all phylogenetic phases (Gilabert 2001). A few of the mechanisms that regulate calcium concentration ($[Ca^{2+}]$) at resting value include calcium inflow and efflux from the extracellular space, Ca^{2+} sequestration towards internal Ca^{2+} stores, Ca^{2+} release from internal Ca^{2+} stores and calcium buffering. Ca^{2+} buffers are among a small number of proteins that bind Ca^{2+} and have acidic side-chain residues. The two primary mechanisms that regulate Ca^{2+} persistence in the cytosol and subsequent Ca^{2+} mediated activities are Ca^{2+} elimination and Ca^{2+} diffusion (Gilabert 2001). Ca^{2+} efflux and sequestration together remove Ca^{2+} from the cytosol, whereas Ca^{2+} diffusion is predominantly regulated by Ca^{2+} buffering. The quick binding of Ca^{2+} to various cellular binding sites when they enter the cytoplasm is known as buffering of Ca^{2+}. Only 1–5% of the Ca^{2+} that enter the cell are thought to remain in its free physiologically active state, making Ca^{2+} buffering an essential step in Ca^{2+}

✉ Vedika Mishra
d20ma001@amhd.svnit.ac.in

Neeru Adlakha
nad@amhd.svnit.ac.in

[1] Department of Mathematics, SVNIT, Gujarat 395007 Surat, India

signaling. It is possible for mobile or immobile buffers to mediate Ca^{2+} buffering at the cytosol which will control the diffusion and confine the movement of free Ca^{2+} inside the cytoplasm. Immobile buffers are represented by molecules that are tethered to intracellular structures or molecules with a high molecular weight. Mobile buffers are compounds with small molecular weights usually less than 20–25 kDa. Ca^{2+} binding capability in mobile buffers is thought to be approximately one-tenth that of the cytosol. ATP is one of the most important transportable Ca^{2+} buffers. Around 2–3 mM of ATP are thought to be present in the cytosol from which 0.4 mM are in a free state. A powerful and extremely portable Ca^{2+} chelator is ATP. Within 10 to 50 nm of the Ca^{2+} entry site, more than 95% of the Ca^{2+} are quickly linked to the buffers. When such elevated $[Ca^{2+}]$ domains occur, a mobile Ca^{2+} buffer will act to disperse them, whereas stationary Ca^{2+} buffers will act to prolong them. The Ca^{2+} binding proteins can be identified as soluble proteins in the cytosol, intraluminal proteins in organelles like the endoplasmic reticulum (ER) or intrinsic proteins in membranes like the plasma or organellar membranes. Physiological processes that rely on Ca^{2+} can be modulated by Ca^{2+} buffering changes that can impact signaling patterns. Phospholipase C (PLC) signaling channels become active when Ca^{2+} signaling is activated. An agonist activates a PLC type (PLCγ or PLCβ) when it interacts with a cell surface receptor. This kind of PLC catalyzes the subsequent breakdown of phosphatidyl inositol bisphosphate (PIP2) into IP_3 and DAG. A brief rise in $[Ca^{2+}]$ results from the release of Ca^{2+} from the IP_3-sensitive Ca^{2+} storage. The activation of a plasma membrane TRPC (T-cell receptor) channel by the second messenger DAG leads to the direct influx of Ca^{2+} into the cytosol. IP3R interacts with the DAG-activated TRPC to contribute to DAG-induced Ca^{2+} influx (Chakrabarti and Chakrabarti 2006).

Calcium signaling has been studied in various cells like neurons, oocytes, myocytes, astrocytes, pancreatic acinars, hepatocytes etc. by various researchers (Jha and Adlakha 2014; Jha et al. 2016; Panday and Pardasani 2013; Jagtap and Adlakha 2019; Kotwani and Adlakha 2017; Manhas and Anbazhagan 2021; Tewari 2012; Manhas and Pardasani 2014a, b; Singh and Adlakha 2019a, b, c). Kotwani et al. have attempted to study one-dimensional calcium concentration variation in fibroblast cells to study the influence of calcium transfer between different cellular compartments, involving excess buffers using the finite difference method (Kotwani and Adlakha 2017). A two-dimensional mathematical model for calcium distribution in fibroblast cells was also developed by them for an unsteady state case. The study was done for two cases of source geometry viz. point source and line source (Kotwani et al. 2014a, b; Kotwani et al. 2014a, b). Panday et al. formulated a model for Ca^{2+} distribution in oocytes involving Na^{+}/Ca^{2+} exchanger (NCX) and advection of Ca^{2+} in the cell (Panday and Pardasani 2013). Naik et al. studied the calcium distribution involving voltage-gated calcium channels(VGCC), ryanodine receptors(RyR) and buffers in oocyte cells. They concluded that the increase of Ca^{2+} concentration due to RyR was higher than that of VGCC (Naik and Pardasani 2015). Amrita et al. observed the effects of NCX, source geometry, leak, SERCA pump etc. on Ca^{2+} oscillations in dendritic spines & neuron cells employing finite element approach (Jha and Adlakha 2014, 2015; Jha et al. 2016; Yripathi and Adlakha 2013). Pathak et al. devised a mathematical model of calcium distribution in cardiac myocyte cells involving pump, excess buffer and leaks (Pathak and Adlakha 2015). Manhas et al. studied calcium variation in pancreatic acinar cells describing the effect of mitochondria on Ca^{2+} signaling (Manhas and Pardasani 2014a, b; Manhas and Anbazhagan 2021; Manhas and Pardasani 2014a, b). Tewari et al. have developed a model for neuron cells expressing the impact of sodium pump on Ca^{2+} oscillation and calcium diffusion with excess buffer (Tewari 2012; Tewari and Pardasani 2012). Jagtap et al. studied calcium variation in a hepatocyte cell using finite volume method. They developed a steady-state one-dimensional mathematical formulation using the advection–diffusion equation for calcium and IP_3 (Jagtap and Adlakha 2019). They also solved the problem for calcium concentration fluctuation in two-dimensions using the finite volume method for the unsteady state situation (Jagtap and Adlakha 2018). Kumar et al. devised a mathematical model to obtain insight through the one-dimensional unsteady state intracellular calcium distribution in T cells. The model takes into account factors like source inflow, buffers, ryanodine receptors (RyRs) and diffusion coefficient (Kumar et al. 2017). Kothiya et al. provided a mathematical model to analyze the effect of Ca^{2+} signaling on the synthesis of ATP and IP_3 in fibroblast cells (Kothiya and Adlakha 2023). The results revealed that variations in source influxes, buffers and diffusion coefficient can alter the production and degradation of ATP and IP_3, resulting in anomalies in fibroblast cells that contribute to cancer, inflammation and wound healing such as cardiac fibroblast cell proliferation and migration (Kothiya and Adlakha 2022). Bhardwaj et al. employed a differential quadrature approach based on radial basis functions to study nonlinear spatio-temporal dynamics of Ca^{2+} in T cells involving the SERCA pump, RyR, source amplitude and buffers (Bhardwaj and Adlakha 2023). Singh et al. developed a mathematical model in one and three dimension for the study of nonlinear IP_3-dependent calcium dynamics in cardiac myocyte (Singh and Adlakha 2019a, b, c; Singh and Adlakha 2019a, b, c; Singh and Adlakha 2019a, b, c). The cytosolic calcium level was found to be potentially regulated by IP_3 signaling, source input of calcium, leak and maximum IP_3 production. Pawar et al. studied the interdependence of calcium and IP_3 using

a two-way feedback model effecting the production of nitric oxide and the production and degradation of β-amyloid in neuron cells. A dopaminergic neuron cell's dopamine control and dysregulation were also analyzed by developing a numerical model (Pawar and Raj Pardasani 2022; Pawar and Pardasani 2022a, b, c; Pawar and Pardasani 2023). Using the system of reaction–diffusion equations for calcium and β-amyloid, the dependency of calcium and β-amyloid in a neuron cell was investigated (Pawar and Pardasani 2022a, b, c). A reaction–diffusion equation system was employed to study the alterations in different factors such as buffer, RyR, SERCA pump, source inflow, etc. which contribute to the regulation and dysregulation of spatio-temporal calcium and NO dynamics in neuron cells (Pawar and Pardasani 2022a, b, c). Vaishali et al. investigated beta cell's response to calcium and IP_3 dynamics in terms of secreting insulin (Vaishali and Adlakha 2023). Yogita et al. analyzed the effects of Ca^{2+} and IP_3 dynamics on glycogen phosphorylase regulation in hepatocyte cells (Jagtap and Adlakha 2023).

Neher et al. studied the buffer and calcium gradient in bovine chromaffin cells. It was concluded that 98–99% of the calcium which typically enter the cell is absorbed by the fast endogenous Ca^{2+} buffer, according to two independent estimates of its capacity (Neher and Augustine 1992). Smith et al. developed asymptotic approximations, including the excess buffer approximation, rapid buffer approximation and immobile buffer approximation to address the steady state problem of buffered diffusion of Ca^{2+} at a single source. In their investigation, they took into account the three-parameter regimes described by the dimensionless diffusion coefficients of Ca^{2+} and buffer with respect to one another and the rate of response (Smith et al. 1996; Smith 1996). Schwaller observed that the impact of a particular Ca^{2+} buffer on intracellular Ca^{2+} signals depends on a variety of variables including intracellular concentration, affinities for Ca^{2+} and other metal ions, the kinetics of Ca^{2+} binding and release in different cells (Schwaller 2019). Martin Falcke used reaction–diffusion equations and developed a mathematical model including calcium concentration, slow buffer, mobile buffer etc. and discovered that a fast buffer's concentration profile around an open channel is more localized than a slow buffer's (Falcke 2003). Nowycky et al. employed diffusion equations and showed that fixed and diffusible calcium buffers affect the spatial and temporal distribution of free Ca^{2+} after Ca^{2+} entrance through voltage-gated ion channels in chromaffin cells (Nowycky and Pinter 1993). Klingauf et al. discussed that the kinetic data from flash-photolysis experiments can be combined with Ca^{2+} data to explain a range of catecholamine secretion-related phenomena from chromaffin cells (Klingauf and Neher 1997). Naraghi et al. presented an explicit solution to a linear approximation of the combined reaction–diffusion problem that takes into consideration of any number of calcium buffers that can be produced naturally or introduced exogenously (Naraghi and Neher 1997). M.D. Stern developed a mathematical model and illustrated that when intracellular processes including the opening and closing of channels, induce rapid fluctuations in calcium fluxes, a buffer with rapid kinetics is required to stabilize the level of $[Ca^{2+}]$ (Stern 1992). Agarwal et al. developed a model incorporating calcium binding buffers and the advection diffusion equation. The impacts on the calcium concentration level were discussed in relation to EGTA, BAPTA, Calmodulin and Troponine (Agarwal et al. 2021). Ahmed et al. investigated the process of Archidoris monteryensis neuron's soma regulating calcium levels and buffers calcium transients at physiological levels. To minimize transient changes in free calcium, measured amounts of intracellular EGTA was used in an indirect technique to measure the cytoplasm's ability to buffer calcium (Ahmed and Connor 1988). Prins et al. discussed the idea that the multifunctionality of organellar Ca^{2+} buffers which exhibit such diversity in their Ca^{2+} binding and reactions, is one feature that unites them. Protein folding, apoptosis control and Ca^{2+} release pathway modulation are just a few of the functions that Ca^{2+} buffering proteins perform in addition in acting as an inactive Ca^{2+} breakdown within intracellular organelles for eukaryotic cells (Prins and Michalak 2011). Faas et al. concluded that the calcium binding protein has one independent and four cooperative binding sites simultaneously, it was also found that calcium binding to calretinin in different cells was a phenomenon due to the reduction of free calcium following significant rise in calcium concentration caused by the release of calcium from DM-nitrophen (Faas et al. 2007). Foehring et al. identified cell break-in over steady state using fluorescent Ca^{2+} μ M fura-2 exogenous buffer stimulating with a single action potential and measured the Ca^{2+} transient from the proximal dendrite for dopamine neurons (Foehring et al. 2009). Gabso et al. showed the effect of cellular Ca^{2+}-buffers on the intensity and diffusional spread of Ca^{2+}-impulses in neurons. Mobile buffers aid in Ca^{2+} redistribution whereas fixed Ca^{2+} buffers tend to delay the signal and lower the measured Ca^{2+} diffusion coefficient (Gabso et al. 1997).

Dysregulation in calcium signaling results in various diseases like obesity, insulin resistance, diabetes etc. Obesity is characterized as a condition in which there is an accumulation of extra body fat that may have a negative impact on health. Obesity in the upper body is characterized by an intra-abdominal accumulation of adipose tissue, this is crucial for the emergence of hypertension, elevated plasma insulin levels, insulin resistance, type 2 diabetes and hyperlipidemia (Kopelman 2000). Excess lipid accumulation is a defining feature of obesity. The WHO BMI (kg/m^2) standards are followed by the majority of definitions of obesity, though other definitions are sometimes used. If a person's BMI is $\geq$ 30 kg/m^2, they are considered fat.

Obesity can range from class 1 (30.0–34.9 kg/m^2) to class 2 (35.0–39.9 kg/m^2) and class 3 (above or equal to 40 kg/m^2) (Montalto 2021). Obesity is a significant contributing factor to increased morbidity and death, especially for diabetes and cardiovascular disease (CVD), cancer and other chronic illnesses like osteoarthritis, liver and kidney disease, sleep apneaspa and depression (Pi-Sunyer 2002).

The survey of literature gives a fair idea that not much attention is given to mathematical modelling to study interdependent calcium and buffer dynamics for a hepatocyte cell. The studies reported above on calcium dynamics have been performed by taking buffer as a constant in their model. The studies on interdependent Ca^{2+} and IP_3, Ca^{2+} and NO, Ca^{2+} and dopamine etc. were reported by taking buffers as constant. But, the concentration of buffers is also dynamic. To obtain better insights, a model of the interdependent Ca^{2+} and buffer dynamics in a hepatocyte cell must be developed. In the present study, a novel two-way reaction–diffusion model for interdependent Ca^{2+} and buffer dynamics has been formulated. The reaction–diffusion equations of Ca^{2+} and buffer have been coupled through their interdependent fluxes. Also, the temporal DAG growth equation has been coupled in this work to analyze the impact of interdependent Ca^{2+} & buffer dynamics on DAG net growth in normal and obese hepatocyte cells. Further, numerical simulation has been performed using the finite element method and the Crank-Nicolson method.

Mathematical formulation

A mathematical model proposed by Smith and Caamal et al. (Smith et al. 1996; Lopez-Caamal et al. 2014) is modified in this study by incorporating IP3R, SERCA pump, RyR and calcium buffering fluxes. The following reaction–diffusion equation for calcium is used for the study

$$\frac{\partial [Ca^{2+}]}{\partial t} = D_{Ca}\frac{\partial^2 [Ca^{2+}]}{\partial x^2} + J_{IPR} + J_{RYR} - J_{SERCA} - J_{on} + J_{off} \tag{1}$$

Here $[Ca^{2+}]$ represents calcium concentration in the cytosol, D_{Ca} is the diffusion coefficient of calcium, J_{IPR} is calcium influx through IP3R, J_{RYR} is calcium influx through RyR, J_{SERCA} is efflux of calcium from SERCA pumps, J_{on} and J_{off} represent Ca^{2+} buffering flux and it's release from the buffers.

The various fluxes are modelled as,

$$J_{IPR} = \frac{K_{IPR}O_{IPR}}{V_c}(CT - (1 + V_c)[Ca^{2+}]) \tag{2}$$

K_{IPR} represents receptor activity levels in the cytosol, CT is total calcium content and V_c is the proportion of cytosol to total cell volume & O_{IPR} is given by (Wacquier et al. 2016),

$$O_{IPR} = \frac{q_{26}}{q_{62} + q_{26}}D \tag{3}$$

Here O_{IPR} represents the open probability of IP3R receptors in the cytosol. q_{26} and q_{62} are transition rate from C_2 to O_6 and transition rate from O_6 to C_2 respectively.

$$D = \frac{q_{42}(q_{62} + q_{26})}{q_{42}q_{62} + q_{42}q_{26} + q_{24}q_{62}} \tag{4}$$

D represents the proportions of the IP3Rs in the cytosol, q_{42} and q_{24} are the transition rates between the modes park to drive and drive to park respectively.

$$J_{RYR} = \frac{V_{RyR}P_O}{V_e}(CT - (V_e + V_c)[Ca^{2+}]) \tag{5}$$

Here P_O is the rate of calcium efflux, V_e is the ratio of ER volume to total cell volume and V_{RyR} is rate of RyR (Naik and Pardasani 2015).

$$J_{SERCA} = \lambda_{SERCA}\frac{[Ca^{2+}]^2}{[Ca^{2+}]^2 + K^2_{SERCA}} \tag{6}$$

Here the bulk cytosol's maximal SERCA flux is λ_{SERCA} and the cytosolic Ca^{2+} concentration of SERCA at half-maximal activation is K_{SERCA} (Wagner et al. 2004).

$$J_{on} = k_j^+[Ca^{2+}]b \tag{7}$$

$$J_{off} = k_j^-\frac{b_{tot}[Ca^{2+}]}{K + [Ca^{2+}]} \tag{8}$$

Here k_j^+ and k_j^- represent the buffer association rate and buffer dissociation rate respectively (Lopez-Caamal et al. 2014; Smith et al. 1996).

Diffusion equation for buffer is given as (Lopez-Caamal et al. 2014),

$$\frac{\partial b}{\partial t} = D_b\frac{\partial^2 b}{\partial x^2} - J_{on} + J_{off} \tag{9}$$

where D_b represents the diffusion coefficient of the buffer, b is buffer concentration in the cytosol, J_{on} and J_{off} are given in Eqs. (7) and (8).

The following initial conditions are imposed based on the assumption that Ca^{2+} and buffer concentration at rest is 0.1 μM and 0 μM in the cell.

$$([Ca^{2+}]_{t=0}) = 0.1\mu M \tag{10}$$

$$(b_{t=0}) = 0\mu M \tag{11}$$

The following boundary conditions based on physical conditions are applied to obtain the solution.

$$lim_{x\to 0} - D_{Ca}\left(\frac{\partial[Ca^{2+}]}{\partial x}\right) = \sigma_{Ca}, \tag{12}$$

where σ_{Ca} represents source influx (Jagtap and Adlakha 2019).

$$lim_{x\to 15}([Ca^{2+}]) = C_{\infty} = 0.1\mu M, \tag{13}$$

$$lim_{x\to 0} D_b\left(\frac{\partial b}{\partial x}\right) = 0, \tag{14}$$

$$lim_{x\to 15}(b) = b_{\infty} = \frac{Kb_{tot}}{K + C_{\infty}}, \tag{15}$$

Here $K=\frac{k^-}{k^+}$ is dissociation constant of the buffer and total buffer concentration is b_{tot} (Patil et al. 2022, Jagtap and Adlakha 2019).

The terms of the various fluxes given in Eqs. (6) and (7) are nonlinear, therefore linearized using the Taylor's approximation method around the point where calcium and buffer concentration is 0.1 and 5 μM. The nonlinear terms in Taylor series approximation becomes negligible.

Rate of DAG net growth is calculated by (Siso-Nadal et al. 2009),

$$\frac{d[DAG]}{dt} = v_i\frac{[Ca^{2+}][PLC^*]}{K_c^{(1)} + [Ca^{2+}]} - b_d[DAG], \tag{16}$$

Here $[DAG]$ represents DAG concentration in the cell, $[PLC^*]$ denotes the concentration of activated PLC β, the rate at which activated PLC can produce IP_3 at its maximal capacity is v_i and $[Ca^{2+}]$ at which this rate is halved is $K_c^{(1)}$.

The Eq. (1) can be rewritten after linearization as,

$$\frac{\partial u}{\partial t} = D_{Ca}\frac{\partial^2 u}{\partial x^2} - A_1 u + B_1 0 \le x \le 15, t \ge 0 \tag{17}$$

where u represents $[Ca^{2+}]$ and A_1 and B_1 are constants obtained after Taylor's approximation method.

In a similar manner representing free buffer concentration as b, Eq. (9) can be rewritten as,

$$\frac{\partial b}{\partial t} = D_b\frac{\partial^2 b}{\partial x^2} - A_2 b + B_2 0 \le x \le 15, t \ge 0 \tag{18}$$

where A_2 and B_2 are constants obtained after Taylor's approximation method.

The numerical solution is obtained by the variational finite element method by dividing the cytosol of the hepatocyte cell into 80 elements. The variational functional of the problem (17) in discretized form is expressed by

$$I^{(e)} = \frac{1}{2}\int_{x_i}^{x_j}\left[u^{(e)'2} + \frac{1}{D_{Ca}}\frac{\partial u^{(e)^2}}{\partial t} + A_1 u^{(e)2} - 2B_1 u^{(e)}\right] - \mu^{(e)}\left(\frac{\sigma_{Ca}}{D_{Ca}}u^{(e)}_{(x=0)}\right) \tag{19}$$

Here $\mu^{(e)}$ is one for the first element and zero for the remaining elements.

The elements are very small in size therefore for calcium concentration shape function is assigned as following linear variation,

$$u^{(e)} = c_1 + c_2 x \tag{20}$$

The Eq. (20) can be expressed as

$$u^{(e)} = P^T C^{(e)} \tag{21}$$

Here $P^T = \begin{bmatrix}1 & x\end{bmatrix}$and

$$C^{(e)} = \begin{bmatrix}c_1\\ c_2\end{bmatrix}$$

Values of $u^{(e)}$ at nodes x_i and x_j are given by,

$$u^{(e)}(x_i) = c_1 + c_2 x_i \tag{22}$$

$$u^{(e)}(x_j) = c_1 + c_2 x_j \tag{23}$$

using above equations, it is obtained as,

$$\overline{u}^{(e)} = P^{(e)}C^{(e)} \tag{24}$$

Here $P^{(e)} = \begin{bmatrix}1 & x_i\\ 1 & x_j\end{bmatrix}$
& $\overline{u}^{(e)} = \begin{bmatrix}u_i\\ u_j\end{bmatrix}$
From Eqs. (22)-(24),

$$u^{(e)} = P^T R^{(e)}\overline{u}^{(e)} \tag{25}$$

Here $R^{(e)} = P^{(e)^{-1}} = \frac{1}{x_j - x_i}\begin{bmatrix}x_j & -x_i\\ -1 & 1\end{bmatrix}$

$$I^{(e)} = I_k^{(e)} + I_m^{(e)} + I_l^{(e)} - I_r^{(e)} - I_s^{(e)}$$

Here

$$I_k^{(e)} = \frac{1}{2}\int_{x_i}^{x_j}\left[\left(P_x{}^T R^{(e)}\overline{u}^{(e)^2}\right)\right]dx$$
$$I_m^{(e)} = \frac{1}{2}\int_{x_i}^{x_j}\frac{1}{D_{Ca}}\frac{\partial}{\partial t}\left[\left(P^T R^{(e)}\overline{u}^{(e)^2}\right)\right]dx$$
$$I_l^{(e)} = \frac{1}{2}\int_{x_i}^{x_j}A_1\left[\left(P^T R^{(e)}\overline{u}^{(e)^2}\right)\right]dx$$
$$I_r^{(e)} = \int_{x_i}^{x_j}B_1\left[\left(P^T R^{(e)}\overline{u}^{(e)}\right)\right]dx$$
$$I_s^{(e)} = \mu^{(e)}\left[\left(\frac{\sigma_{Ca}}{2D_{Ca}}P^T R^{(e)}\overline{u}^{(e)}_{(x=0)}\right)\right]$$

Minimizing $I^{(e)}$ with respect to $\overline{u}^{(e)}$,

$$\frac{dI^{(e)}}{d\overline{u}^{(e)}} = 0$$

that is,

$$\frac{dI^{(e)}}{d\overline{u}^{(e)}} = \frac{dI_k^{(e)}}{d\overline{u}^{(e)}} + \frac{dI_m^{(e)}}{d\overline{u}^{(e)}} + \frac{dI_l^{(e)}}{d\overline{u}^{(e)}} - \frac{dI_r^{(e)}}{d\overline{u}^{(e)}} - \frac{dI_s^{(e)}}{d\overline{u}^{(e)}}$$

which can be written as,

$$\frac{dI}{d\overline{u}^{(e)}} = \sum_{e=1}^{80} \overline{M}^{(e)} \frac{dI^{(e)}}{d\overline{u}^{(e)}} (\overline{M}^{(e)})^T = 0$$

where

$$\overline{M}^{(e)} = \begin{bmatrix} 0 & 0 \\ . & . \\ 0 & 0 \\ 1 & 0 \\ 0 & 1 \\ 0 & 0 \\ . & . \\ 0 & 0 \end{bmatrix}_{81\times 2} \begin{matrix} \\ \\ \\ i^{th} row \\ j^{th} row \\ \\ \\ \\ \end{matrix}, \quad \overline{u}^{(e)} = \begin{bmatrix} u_1 \\ u_2 \\ u_3 \\ u_4 \\ . \\ . \\ u_{80} \\ u_{81} \end{bmatrix}_{81\times 1}$$

In a similar manner Eq. (18) is solved using linear elements leading again to an 81×81 system.

This results in the set of linear algebraic equations,

$$[\overline{K}]_{(162\times 162)}\overline{U} + [\overline{N}]_{(162\times 162)} \frac{\partial \overline{U}}{\partial t}_{(162\times 1)} = [\overline{F}]_{(162\times 1)} \qquad (26)$$

where $\overline{U}$ is given by $\begin{bmatrix} \overline{u} \\ \overline{B} \end{bmatrix}$, system matrices are represented as $\overline{K}$ and $\overline{N}$ & $\overline{F}$ is characteristic vector. For solving the system Crank-Nicolson method is used and simulated using MATLAB program.

Table

The following physiological parameters are used for solving the formulated problem (26).

Results & discussion

Figure 1 displays calcium and free buffer concentration distribution with respect to space and time. Figure 1A shows spatial calcium concentration fluctuations. The figure displays that the concentration of calcium is highest near the source which decreases to reach equilibrium value on moving away from the source. Highest steady state concentration of calcium is close to ≈ 0.7 Mμ. Figure 1B shows the concentration of calcium variation with respect to time. Initially, the concentration of calcium increases sharply till 500 ms and then attains a steady state. Figure 1C shows free buffer concentration variation with respect to space. Free buffer binds with free calcium to form calcium-bound buffer because excessive amount of calcium is harmful to cells. Near the source, the concentration of calcium is highest therefore more amount of buffer is needed to reduce the concentration of calcium. Hence, the free buffer value is smallest near the source. Buffer diffuses to the calcium source whereas calcium diffuses toward the other end of the cell. Thus near the source influx of free calcium, it is observed that source influx dominates the buffering process while on the other end of the boundary, the buffering process dominates over calcium signals. Figure 1D shows free buffer concentration variation with respect to time. Initially, free buffer concentration increases gradually and smoothly till 500 ms and then attains steady state. The maximum steady state value of the buffer is observed to be 6.667 μM.

Figure 2 displays calcium concentration distribution with respect to space and time for dynamic and constant buffer values. For the purpose of comparison, the constant buffer value is taken as the maximum steady state value i.e. 6.667 μM as obtained in Fig. 1. Figure 2A shows spatial calcium concentration fluctuations for dynamic and

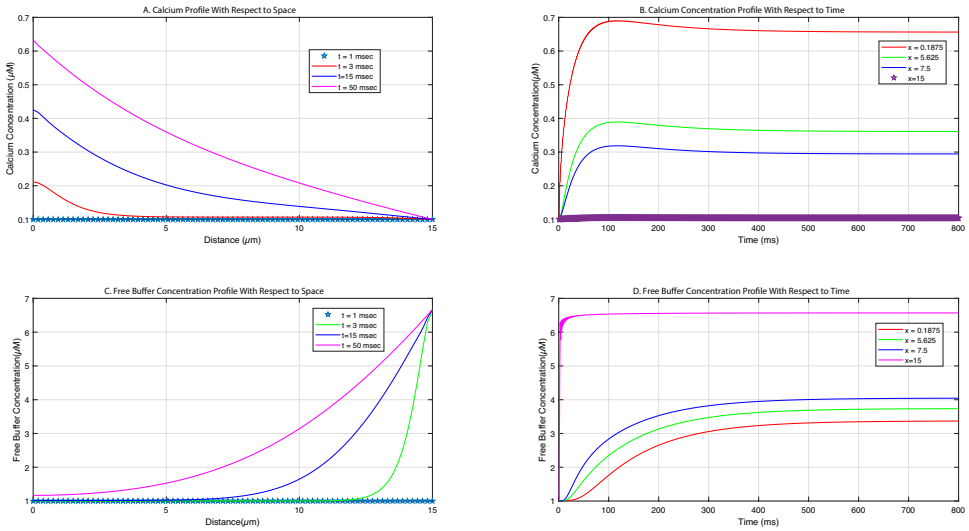

Fig. 1 Calcium and free buffer distribution with $\sigma_{Ca} = 15$ pA, $D_{Ca} = 200\ \mu m^2 sec^{-1}$ and $D_b = 75 = \mu m^2 sec^{-1}$

constant buffer values. It displays that the concentration of calcium is highest near the source which decreases to reach equilibrium value on moving away from the source. It is observed from the Fig. 2A that dynamic buffer is dominated by constant buffer as seen in the plot because constant buffer drops calcium concentration drastically near the source while dynamic buffer gradually decreases calcium concentration and therefore, smoother curve is observed for dynamic buffer. Figure 2B shows concentration of calcium variation with respect to time for dynamic and constant buffer values. Initially, concentration of calcium increases sharply till 300 ms, in case of constant buffer value and then it attains steady state around 300 ms. But in the presence of dynamic buffer, calcium concentration increases sharply till 500 ms and attains steady state thereafter 500 ms. The case of constant buffer is an idealistic situation whereas the case of dynamic buffer represents more realistic situation. Slight oscillations are observed in the curves because of time gap between free calcium and buffers diffusing towards each other and the binding time required to form buffer bound calcium reducing free calcium and buffer concentration. It is observed from the Fig. 2 A and B that in the presence of dynamic buffer value, it almost uniformly reduces concentration of calcium in the entire domain whereas in the presence of constant buffer value, the concentration of calcium reduces drastically which is possible in an ideal case only. Difference of calcium concentration in the cytosol of the cell in the presence of dynamic and constant buffer value is $\approx 30\%$. The significant difference is observed in calcium concentration profile for idealistic and realistic scenario of buffer.

Figure 3 displays changes in calcium concentration for various calcium diffusion coefficient values with respect to time and space. Figure 3A is plotted for spatial variations in calcium concentration. It is observed that with increasing values of the diffusion coefficient of calcium, calcium concentration decreases. Calcium diffusion rises as the value of the diffusion coefficient rises, hence the concentration of calcium is inversely proportional to the diffusion coefficient. Near the source calcium concentration is highest and moving away from the source attains its equilibrium state. Figure 3B shows calcium concentration variation with respect to time. Initially, calcium concentration increases sharply till 300 ms and then attains a steady state. Slight oscillations are observed in the curves because of the time gap between free calcium and free buffers diffusing towards each other and the binding time required to form buffer-bound calcium reducing free calcium and free buffer concentration.

Figure 4 shows a change in calcium concentration for various buffer's diffusion coefficient values with respect to space and time. Figure 4A is plotted for variations in calcium concentration with respect to space. It is observed that with increasing values of the diffusion coefficient of buffer, calcium concentration decreases. Buffer diffusion increases with an increase in diffusion coefficient, which increases the formation of buffers that are calcium-bound. Near the source, calcium concentration is highest and moving away from the source attains its equilibrium state. Figure 4B shows calcium concentration variation with respect to time. Initially, calcium concentration increases sharply till 300 ms and then attains a steady state. Slight oscillations are observed in the curves because of the time gap between free calcium and free buffers diffusing towards each other and the binding time required to form buffer-bound calcium reducing free calcium and buffer concentration.

Figure 5 shows variation in buffer concentration for different buffer's diffusion coefficient values with respect to space and time. Figure 5A demonstrates spatial buffer

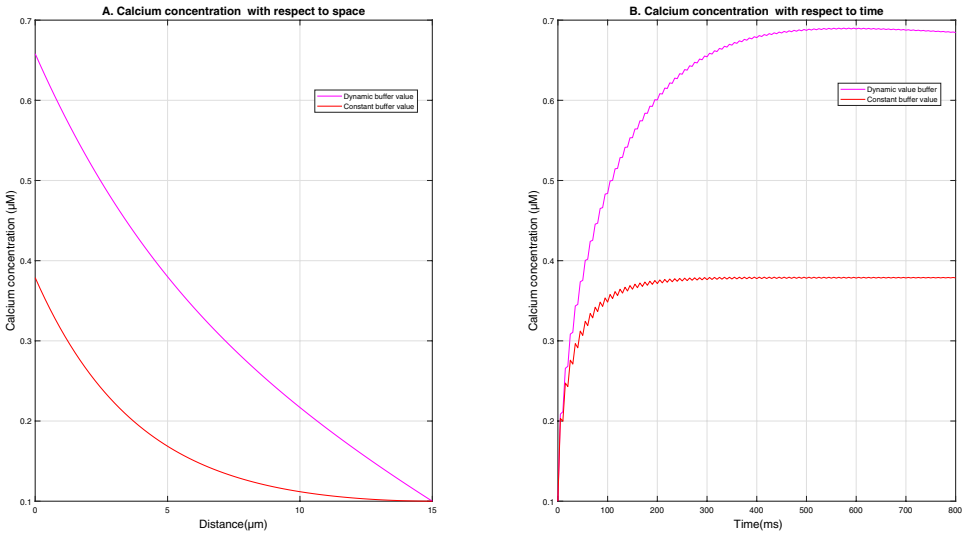

Fig. 2 Calcium dynamics for dynamic and constant buffer with $\sigma_{Ca} = 15\ pA$, $D_{Ca} = 200\ \mu m^2 sec^{-1}$ at 500 ms

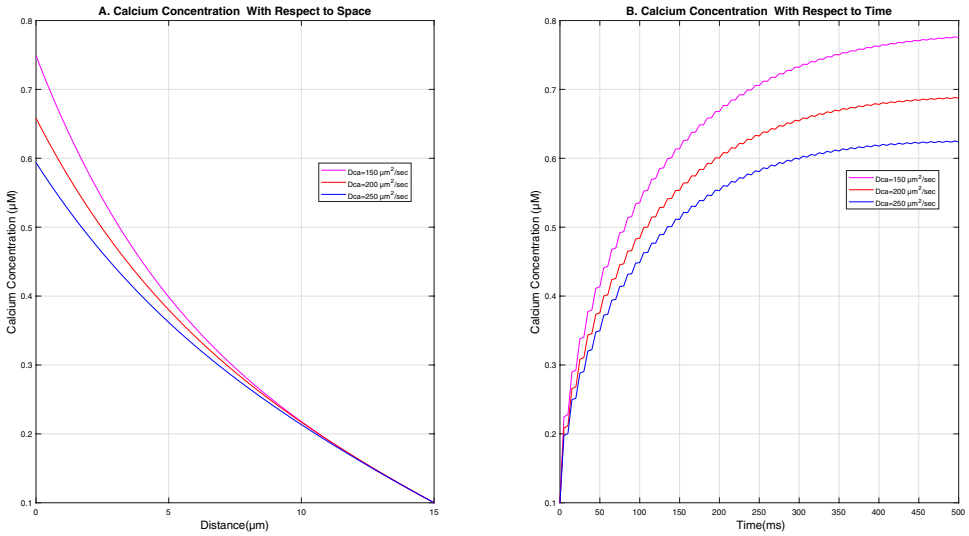

Fig. 3 Calcium dynamics for different values of calcium's diffusion coefficient

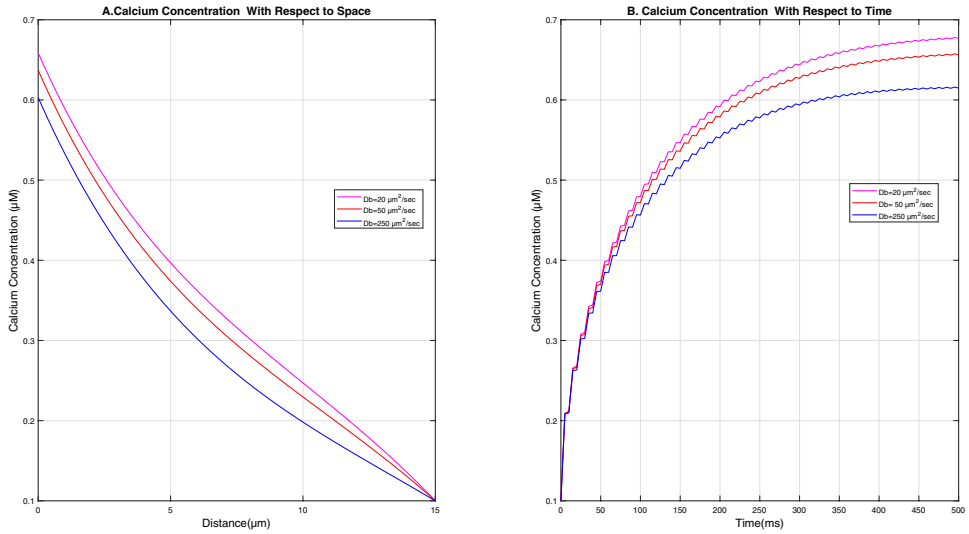

Fig. 4 Calcium dynamics for various levels of the buffer's diffusion coefficient

concentration for various buffer diffusion coefficient values. It is seen from the figure that with increasing value of diffusion coefficient of buffer, buffer concentration in the cytosol of the cell increases as diffusion of buffer increases. At the source calcium concentration is highest, to reduce the concentration of calcium buffer concentration has increased at the source. Figure 5B shows buffer concentration for different values of the buffer's diffusion coefficient with respect to time. Initially, buffer concentration increases gradually up to 30 ms then oscillates for some time around 30 ms to 350 ms (maximum time period) and attains a steady state. Oscillations remain for the maximum time period with increasing the buffer's diffusion coefficient.

Figure 6 displays variations in calcium concentration for various levels of source influx with respect to space and time. Figure 6A is plotted for calcium concentration variation with respect to space. It has been found that calcium concentration rises with rising calcium source inflow values. Near the source calcium concentration is highest and on moving away from the source attains its equilibrium state. Figure 6B shows calcium concentration variation with respect to time. Initially, calcium concentration increases sharply till 400 ms and then reaches a steady state. The calcium concentration variation has the same behavior as seen in Fig. 1.

Figure 7 displays variations in calcium concentration for various total buffer concentration values with respect to space and time. Figure 7A is plotted for calcium concentration variation with respect to space. Calcium concentration is seen to decrease with increasing total buffer concentration levels. With the increase in the total value of buffer, the quantity of calcium-bound buffer increases, hence calcium concentration decreases. Near the source calcium concentration is highest and moving away from the source attains its

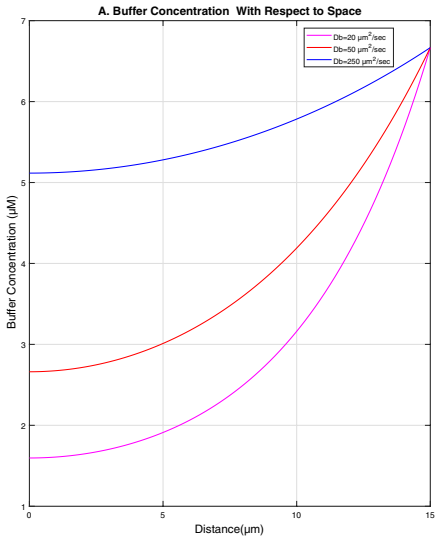

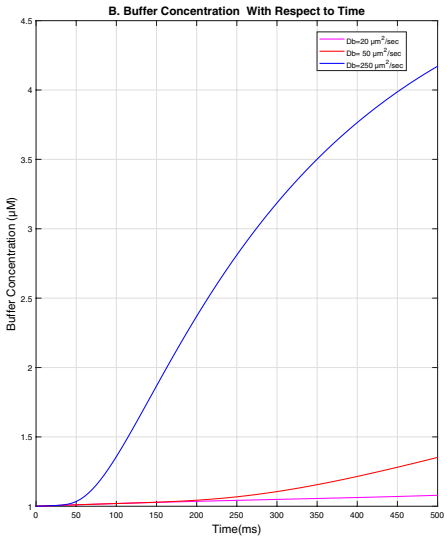

Fig. 5 Buffer dynamics for different diffusion coefficient values of the buffer

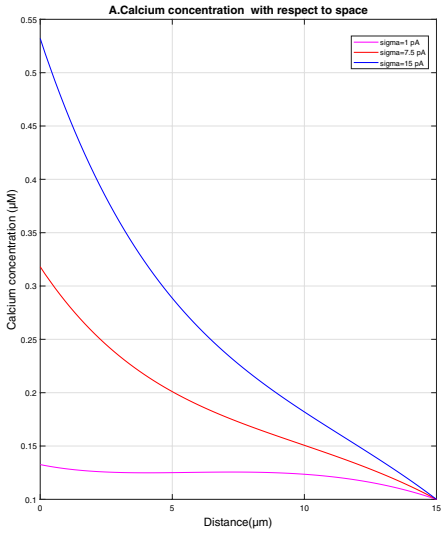

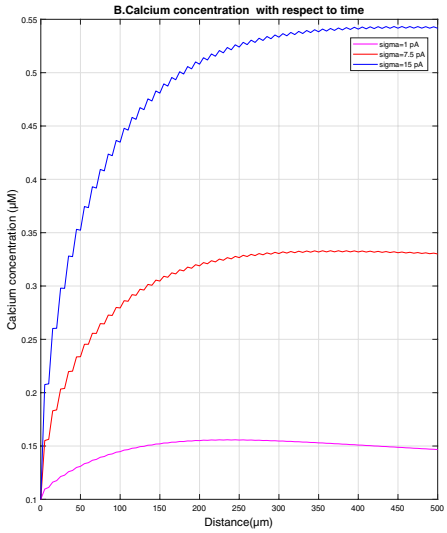

Fig. 6 Calcium dynamics for different values of source influx

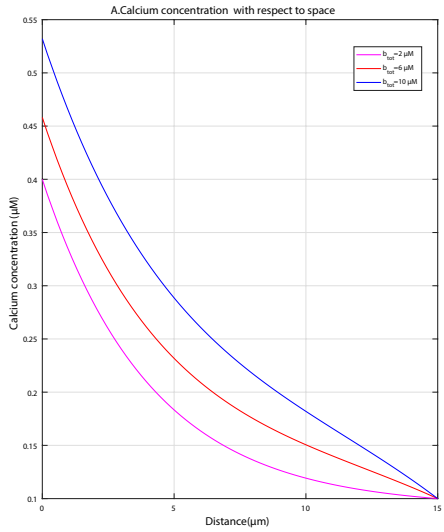

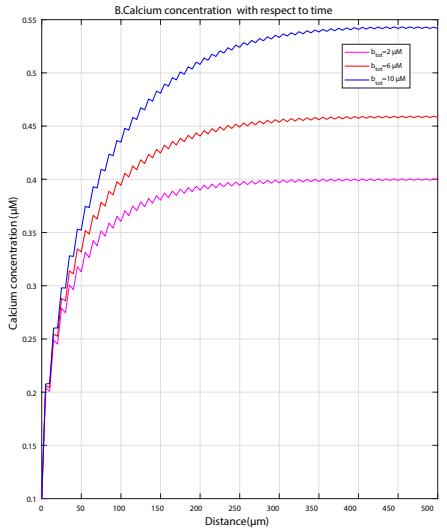

Fig. 7 Calcium dynamics for various values of b_{tot}

equilibrium state. Figure 7B shows calcium concentration variation with respect to time. Initially, calcium concentration increases sharply till 350 ms and then reaches a steady state. Behavior of calcium concentration variation is the same as seen in Fig. 1. Slight oscillations are observed with increasing value of source influx.

Figure 8 shows variations in buffer concentration at various total buffer concentration levels with respect to space and time. Figure 8A displays the fluctuation in buffer concentration with respect to space for various total buffer concentration values. The figure demonstrates that when the overall buffer concentration is at its maximum, the value of the buffer is highest. Additionally, at the source, the buffer reaches a fixed value in less time compared to the scenario where the total buffer concentration is low. Figure 8B shows variation in buffer concentration for different values of total buffer concentration with respect to time. It is seen that buffer starts from a fixed value of 0 μM then initially decreases near the source and then increases with an increase in time.

Figure 9 demonstrates the fluctuation in calcium concentration along time and space for dissociation constants of different buffers which are EGTA, Triponin C and BAPTA. Figure 9A shows calcium concentration variation with respect to space. Upon comparison of calcium concentrations at the source, it is observed that the presence of an EGTA buffer results in the highest calcium concentration, surpassing the concentrations observed with Troponin C and BAPTA. The behavior of the calcium concentration is similar to Fig. 1A in the presence of EGTA buffer. Presence of Triponin C reduced the concentration at the source ≈ by 5% and the BAPTA buffer changed the behavior of the curve. Calcium concentration is highest at the source and decreases as one moves

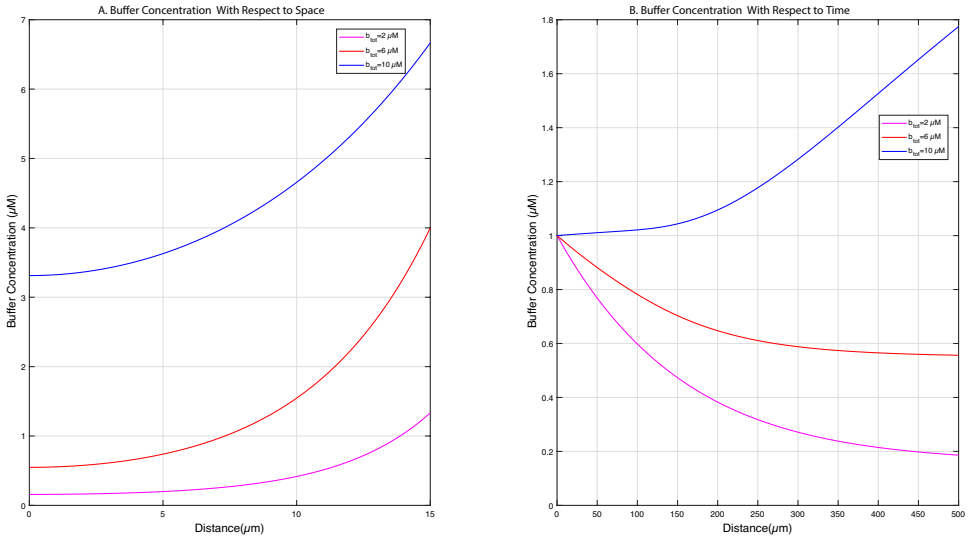

Fig. 8 Buffer dynamics for various total buffer concentration values

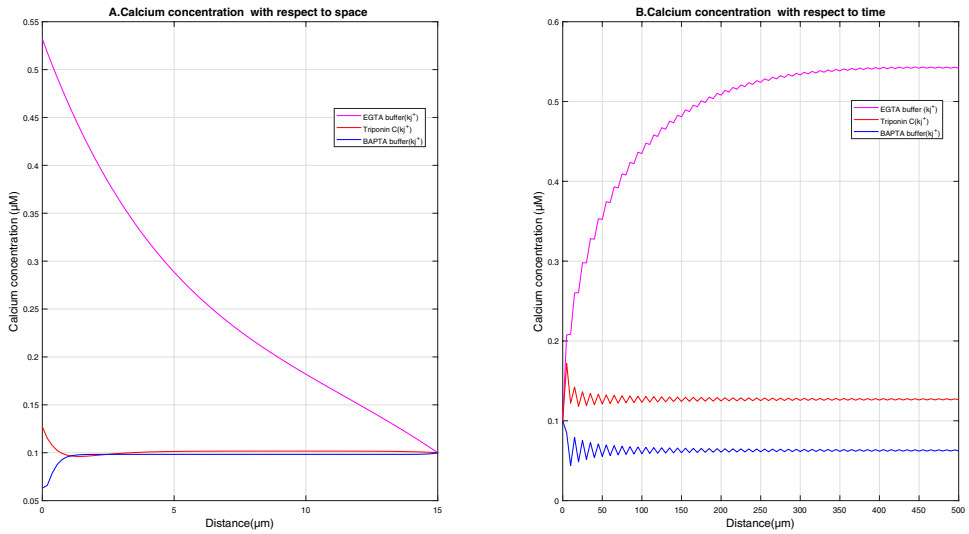

Fig. 9 Calcium dynamics for different values of various buffer association rates

away from the source until it achieves a steady state when EGTA and Triponin C is present. Calcium concentration first rises in the presence of BAPTA buffer for a while before reaching a steady state. Figure 9B shows calcium concentration variation with respect to time. It is seen that in the presence of EGTA, initially, calcium concentration increases sharply and gradually till 350 ms and then attains a steady state. When Triponin C and BAPTA buffers are present steady state is attained in 30 ms. With respect to time, oscillations appear when Triponin C and BAPTA buffers are present.

Figure 10 shows the spatial and temporal DAG net growth rate. Figure 10A shows spatial DAG net growth rate. From the Fig. 10A, it is seen that close to the source, DAG net growth rate is largest and moving away from the source, DAG net growth rate decreases to a certain fixed value. There is a change in the nonlinear behavior of the curve compared to that in Fig. 1A. Figure 10B shows DAG net growth rate with respect to time. It is seen from the curves that the net growth rate increases more gradually and smoothly compared to the temporal calcium profile in Fig. 1B.

Figure 11 displays DAG net growth rate distribution with respect to space and time for dynamic and constant buffer values. Figure 11A shows spatial DAG net growth rate for dynamic and constant buffer values. It displays that the DAG net growth rate is highest near the source which decreases to reach equilibrium value on moving away from the source. It is observed from the Fig. 11A that dynamic buffering is dominated by constant buffering process as seen in the plot because constant buffer drops DAG net growth rate drastically near the source while dynamic buffer gradually decreases DAG net growth rate and therefore, smoother curve is observed for dynamic buffering process. Figure 11B

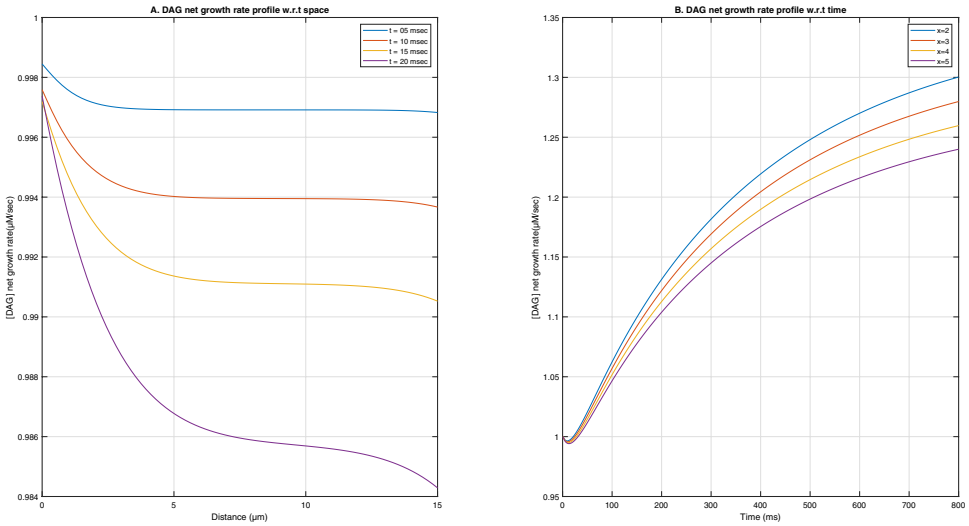

Fig. 10 DAG concentration net growth

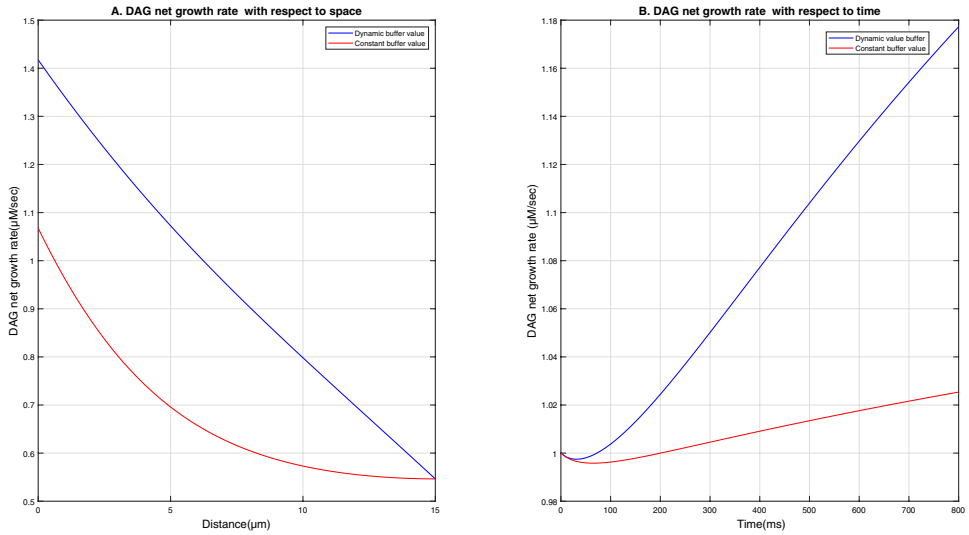

Fig. 11 DAG net growth rate for dynamic and constant buffer with $\sigma_{Ca} = 15\ pA$, $D_{Ca} = 200\ \mu m^2 sec^{-1}$

shows DAG net growth rate with respect to time for dynamic and constant buffer values. DAG net growth rate increases gradually for both the cases dynamic and constant buffer values. It is observed from the Fig. 11A and B that in the presence of dynamic buffer value, it almost uniformly reduces DAG net growth rate in the entire domain whereas in the presence of constant buffer value, the DAG net growth rate reduces drastically which is possible in an ideal case only. Difference of DAG net growth rate in the cytosol of the cell in the presence of dynamic and constant buffer value is ≈ 30%. The significant difference is observed in DAG net growth rate for idealistic and realistic scenario of buffer.

Figure 12 displays a difference of calcium concentration variation from obese hepatocyte cells to normal hepatocyte cells with respect to space and time. Figure 12A shows a spatial difference graph for calcium concentration variation due to obese and normal hepatocyte cells. The graph shows that the difference in calcium concentration from an obese to a normal hepatocyte cell is largest close to the source and gradually reduces as one moves away from the source and becomes zero as calcium concentration attains an equilibrium state in both obese and normal hepatocyte cells. Figure 12B shows a temporal difference graph for calcium concentration variation. The Fig. 12B shows that the behaviour of the fluctuation in calcium concentration is similar to Fig. 1B. Initially, difference in calcium increases upto 400 ms then attains steady state at 400 ms.

Figure 13 shows a difference of DAG net growth rate variation due to obese and normal hepatocyte cells with respect to space and time. Figure 13A shows a spatial difference graph for DAG net growth rate variation. The graph illustrates that the initial difference in calcium concentration near the source increases and reaches its peak at approximately 5 μ m then starts decreasing due to obese and normal

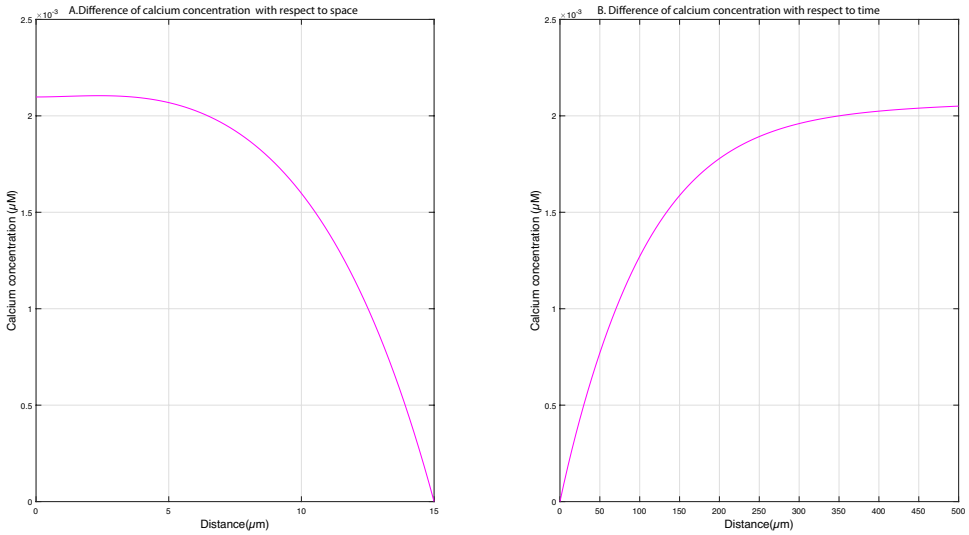

Fig. 12 Difference of calcium concentration due to obese and normal hepatocyte

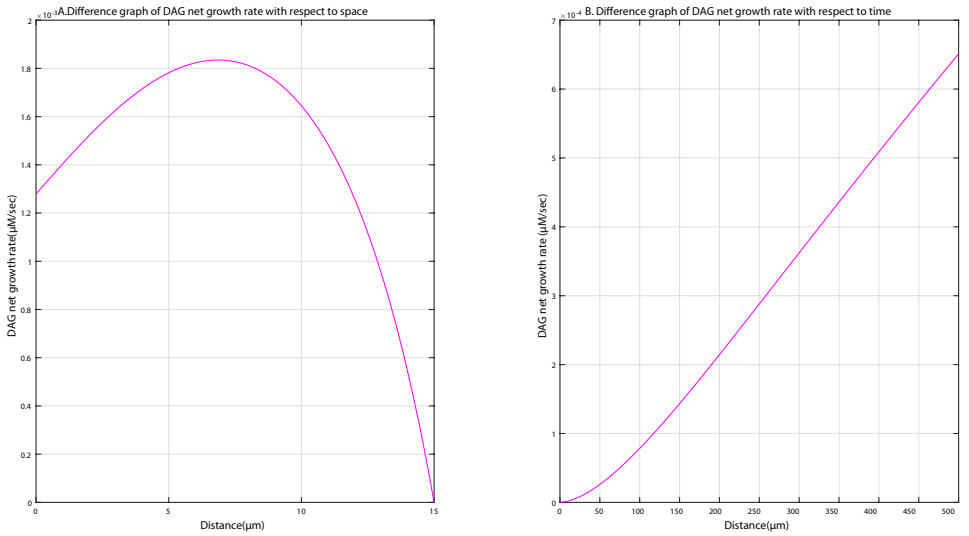

Fig. 13 Difference of DAG net growth rate due to obese and normal hepatocyte

hepatocyte cells and becomes zero. Figure 13B shows a temporal difference graph for DAG net growth rate variation. It is noticed from the figure that the behaviour of the DAG net growth rate variation is similar to Fig. 10B. It is seen from the curves that the difference in net growth rate increases more gradually and smoothly compared to the temporal calcium profile in Fig. 1B

Figure 14 displays calcium concentration distribution in normal and obese hepatocyte cells. Figure 14A shows calcium concentration variation with respect to space for normal and obese cells. The Fig. 14A demonstrates that the concentration of calcium increases in obese cells as ER becomes leaky in obesity. Figure 14B shows calcium concentration variation with respect to time for normal and obese cells. The behaviour of the curves is similar to that in the Fig. 1B.

Figure 15 shows DAG net growth rate variation in normal and obese hepatocytes. Figure 15A shows DAG net growth rate variation with respect to space for normal and obese cells. It is observed from the figure that the DAG net growth rate is high in the case of obese cells. DAG net growth rate is highest at the source. When going away from the source DAG net growth rate decreases and attains a fixed value that is $\approx 0.6\ \mu$ M sec^{-1}. Figure 15B shows DAG net growth rate variation along time. It is observed that initially difference in DAG net growth rate in the obese and normal cells was not much but as time increases difference increases. It is noticed that in obese hepatocyte cells, DAG net growth rate increases in comparison to normal hepatocyte cells.

Figure 16 shows a 3-d plot among calcium concentration, buffer concentration and time at $x = 0$, 0.1875, 0.9375 and 1.6875 mμ. The figure illustrates that the concentration of calcium is a maximum $\approx 0.5\ \mu M$ and the buffer value is smallest

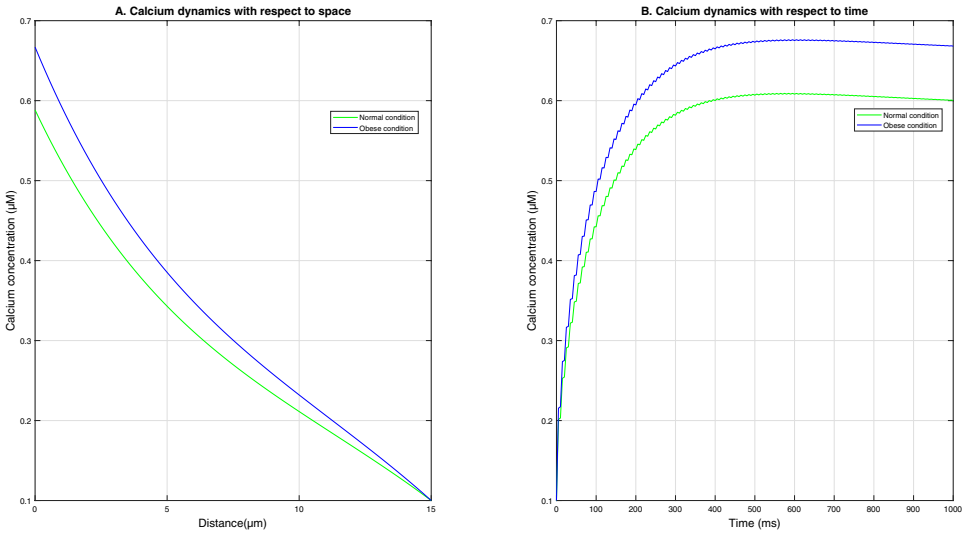

Fig. 14 Calcium concentration variation in normal and obese hepatocyte

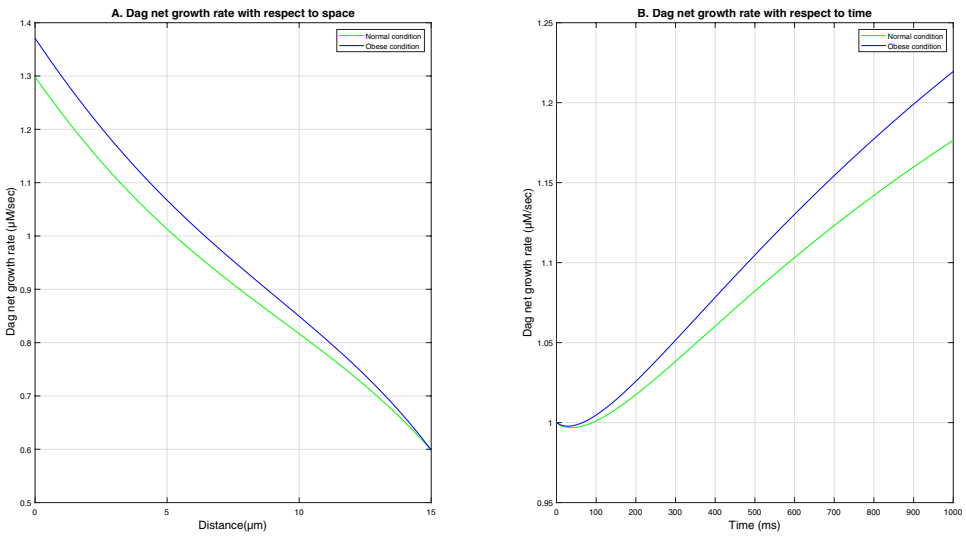

Fig. 15 DAG net growth rate variation in normal and obese hepatocyte

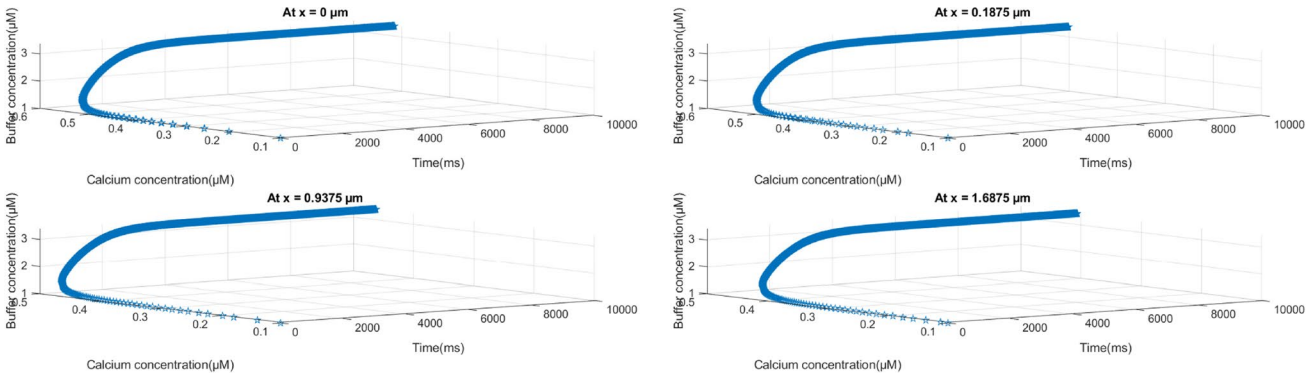

Fig. 16 Graph among calcium and buffer concentrations and time at different spatial positions

Table 1 Physiological parameters for calcium and buffer variation (Jagtap and Adlakha 2019; Smith et al. 1996)

Symbol	Parameter	Value
D_{Ca}	Diffusion coefficient of calcium	200 $\mu m^2/sec$
D_b	Buffer's diffusion coefficient	75 $\mu m^2/sec$
C_∞	Calcium concentration at equilibrium	0.1 μM
V_c	Volume of the cytosol to the total cell volume ratio	0.83
K_{IP3R}	Dissociation constant of activating IP_3 binding site	0.3 μM
CT	Total calcium concentration	2 μM
V_e	Volume of ER relative to total cell volume	0.17
V_{RyR}	RyR rate	0.5 $\mu M/Sec$
Po	Rate of calcium efflux	0.5 M/sec
K_{SERCA}	Half maximal rate of SERCA	0.1 μM
k_j^+	Buffer(EGTA) association rate	1.5 $(\mu M/s)^{-1}$
k_j^-	Buffer(EGTA) dissociation rate	0.3 s^{-1}
b_{tot}	Total buffer concentration	10 μM
λ_{SERCA}	Flux rate of SERCA pump	0.65 s^{-1}

around 0 μM at time t = 0 ms. With the increase in time, calcium concentration reaches its equilibrium value i.e. 0.1 μM and buffer value increase with the increase in time. An inverse relationship is observed between calcium and buffer. As a high quantity of calcium is toxic to the cell, buffers bind with calcium and form a calcium-bound buffer. Therefore, when calcium concentration is high, the free buffer value will be low and when the buffer value is high, calcium concentration will attain a small value (Tables 1, 2, and 3).

Figure 17 shows a 3-d plot of calcium concentration, buffer concentration and time at x=0 mμ for the source influx's different values. It is analyzed from figure that at t=0 ms the concentration of calcium is highest ≈ 0.5 μM and the buffer value is smallest around 0 μM. With the increase in time,

Table 2 Physiological parameters for the comparative study of normal and obese hepatocyte cells (Han and Periwal 2019)

Symbol	Value in normal cell	Value in obese cell
K_{IP3R}	0.15 μM	0.35 μM

calcium concentration reaches its equilibrium value i.e. 0.1 μM and buffer value increases with the increase in time. With the increase in the value of source influx, a gradual and smooth increase in the concentration of buffer is observed with respect to time. The concentration of calcium increases with an increase in source influx, hence buffers take more time to form a calcium-bound buffer. An inverse relationship is observed between calcium and buffer. As a high quantity of calcium is toxic to the cell, buffers bind with calcium and form a calcium-bound buffer. Therefore, when calcium concentration is high, the free buffer value will be low and when the buffer value is high, calcium concentration will attain a small value.

Error and stability analysis

Error analysis is done for t= 0.1, 0.2, 0.3, 0.4 and t=0.5 s at x =0. The finite element method is found effective in this problem as accuracy with 80 linear elements for calcium profile is found as 99.96% and for buffer profile accuracy is 99.47% as displayed in Table 4. The spectral radius for the finite element method is 0.9959 which is less than one therefore, the method is stable.

Validation

The concentration profiles of $[Ca^{2+}]$ obtained for the parameter values taken by Smith et al. (Smith et al. 1996) at x = 0, 0.5, 1, 2 and 15 mμ, are compared to earlier research by Smith et al. (Smith et al. 1996) at time t = 50 s and findings are in good accord, as demonstrated in Table 5.

Table 3 Error analysis for calcium profile with 80 elements and 90 elements

Time	Node = 80	Node = 90	Absolute error	Relative error	Relative % error
0.1 s	0.434841234	0.434658855	0.000182379	0.000336715	0.033671525
0.2 s	0.507936181	0.507725107	0.000211074	0.000389693	0.038969333
0.3 s	0.533282388	0.533072269	0.000210119	0.00038793	0.038793029
0.4 s	0.540837526	0.540640737	0.000196789	0.00036332	0.036332048
0.5 s	0.541640878	0.541462618	0.00017826	0.000329111	0.032911103

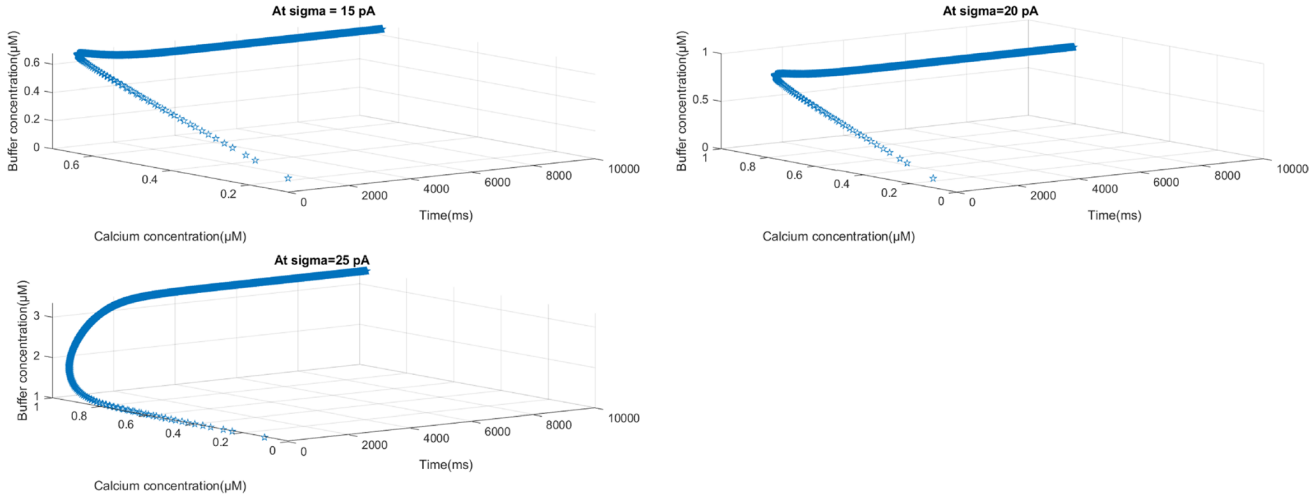

Fig. 17 Graph among calcium and buffer concentrations and time at x = 0

Table 4 Error analysis for buffer concentration profile with 80 elements and 90 elements

Time	Node = 80	Node = 90	Absolute error	Relative error	Relative % error
0.1 s	6.417647309	6.451990997	0.034343688	0.005251473	0.525147303
0.2 s	6.47123838	6.495452231	0.024213851	0.003702526	0.370252553
0.3 s	6.497341311	6.517228151	0.019886839	0.003040885	0.304088479
0.4 s	6.513075094	6.529005888	0.015930794	0.002435968	0.243596831
0.5 s	6.523755814	6.539819997	0.016064183	0.002456365	0.245636468

Table 5 Validation of calcium dynamics with Smith et al. at t = 50 s (Smith et al. 1996)

Distance	Ca^{2+} (Smith)	Ca^{2+} (Present work)	Absolute error	Relative % error
x = 0 μm	0.302433473	0.30123763	0.001195844	0.396976925
x = 0.5 μm	0.260661503	0.258604315	0.002057187	0.682911855
x = 1 μm	0.249294538	0.247739235	0.001555303	0.516304519
x = 2 μm	0.23002896	0.231480878	0.001451918	0.481984222
x = 15 μm	0.1	0.1	0	0

Conclusion

The existing model (Smith et al. 1996; Lopez-Caamal et al. 2014) is modified by incorporating IP3R, SERCA pump, RyR and calcium buffering fluxes and reaction term to propose a new system dynamics model for numerical simulation of calcium, buffer and DAG dynamics due to obese and normal hepatocyte cells. The outcomes were discovered to be consistent with cellular biological phenomena (Naraghi and Neher 1997; Neher and Augustine 1992; Smith et al. 1996). The results lead to the following basic conclusions:

(i) As source inflow increases, it also raises the concentration of free calcium.
(ii) With an increase in free buffer concentration, free calcium concentration falls.
(iii) With an increase in calcium's diffusion coefficient, free calcium concentration drops.
(iv) (iv)The concentration of free calcium decreases as the buffer's diffusion coefficient rises.
(v) Near the source, the concentration of the calcium is largest and calcium diffuses towards other end of the cell ($x = 15\ \mu m$) and reaches an equilibrium state, whereas free buffer concentration diffuses towards calcium source.
(vi) Free calcium and buffer reach at steady state at the same time period with a slight change in temporal behaviour.

The analysis of numerical results leads to the following novel conclusions:

(i) The spatial locations where calcium concentration is high, there consequently the free buffer concentration is low because free buffer concentration decreases due to high buffering activity to lower the free calcium concentration at those locations.
(ii) The spatial locations where the rise in calcium concentration is high, there consequently rise in free buffer concentration is slower because most of the free buffer binds with free calcium. Similarly, wherever buffer concentration is rising rapidly consequently calcium concentration rises slowly.
(iii) Free calcium and free buffer are interdependent depending on their domination at various locations.
(iv) Free calcium and free buffer fluctuate dynamically concerning one another based on the rate of a gradual rise in buffer activity. The difference in calcium profile and DAG net growth rate due to realistic dynamic buffering process and idealistic constant buffering process is quite significant. Thus, it implies that the proposed model provides more realistic simulation results as compared to the existing models.
(v) Due to an increase in calcium-elevating mechanisms brought on by obesity, the amount of free calcium concentration is higher in the obese cell than it is in the normal hepatocyte cell.
(vi) DAG growth rate is higher in obese cells as compared to normal hepatocyte cells due to increase in calcium concentration causing an increase in DAG net growth rate in obese cells.
(vii) The effect of changes in parameters like source, total buffer concentration, SERCA pump etc. on calcium profiles is transferred in a synergistic manner to the net growth rate of DAG. Thus changes in these parameters cause significant changes in the net growth rate of DAG leading to various disorders of the liver like obesity, diabetes etc.
(viii) Obese mice's liver cells had an ER content that was 50% lower. The obesity-related aberrant increase in MAM (mitochondria associated membrane) production induces increased Ca^{2+} flow from the ER to the mitochondria (Arruda et al. 2014). As a result, only a 10% increase in the calcium content of a hepatocyte cell's cytoplasm was anticipated, the same is evident in Fig. 14.

Thus proposed model is quite effective in estimating the levels of concentration of calcium in obesity and normal conditions of the cell. The numerical approach consisting of finite element and Crank- Nicolson method is competent enough to solve the proposed model for generating useful results. The ensuing model excels among others as it is able to incorporate the effect of dynamic variations in free buffer concentration on free calcium concentration and vice versa in normal and obese hepatocyte cells and provide the more realistic dynamics of calcium and buffers in these cells. Similar models can be developed further for other liver disorders like diabetes etc. to generate crucial information for therapeutic applications.

Author contribution As far as problem formulation, data correction, literature review, solution and interpretation of results is concerned both authors own equal responsibility. Author (1) has deduced the results and devised the MATLAB program.

Data availability Not applicable.

Declarations

Conflict of interest There are no conflict of interest in this work.

References

Agarwal R, Kritika, Purohit SD (2021) Mathematical model pertaining to the effect of buffer over cytosolic calcium concentration distribution. Chaos, Solitons Fractals 143:110610. https://doi.org/10.1016/j.chaos.2020.110610

Ahmed Z, Connor JA (1988) Calcium regulation by and buffer capacity of molluscan neurons during calcium transients. Cell Calcium 9(2):57–69. https://doi.org/10.1016/0143-4160(88)90025-5

Arruda AP, Pers BM, Parlakgül G, Güney E, Inouye K, Hotamisligil GS (2014) Chronic enrichment of hepatic endoplasmic reticulum-mitochondria contact leads to mitochondrial dysfunction in obesity. Nat Med 20(12):1427–1435. https://doi.org/10.1038/nm.3735

Bhardwaj H, Adlakha N (2023) Radial basis function-based differential quadrature approach to study reaction-diffusion of Ca^{2+} in T lymphocyte. Int J Comput Methods. https://doi.org/10.1142/s0219876222500591

Chakrabarti R, Chakrabarti R (2006) Calcium signaling in non-excitable cells: Ca^{2+} release and influx are independent events linked

to two plasma membrane Ca^{2+} entry channels. J Cell Biochem 99(6):1503–1516. https://doi.org/10.1002/jcb.21102

Dupont G, Combettes L, Bird GS, Putney JW (2011) Calcium oscillations. Cold Spring Harbor Perspect Biol 3(3). https://doi.org/10.1101/cshperspect.a004226. [accessed 2020 Sep 9]. https://www.ncbi.nlm.nih.gov/pmc/articles/PMC3039928/

Faas GC, Schwaller B, Vergara JL, Mody I (2007) Resolving the fast kinetics of cooperative binding: Ca^{2+} buffering by Calretinin. Aldrich RW, editor. PLoS Biol 5(11):e311.https://doi.org/10.1371/journal.pbio.0050311

Falcke M (2003) Buffers and oscillations in intracellular Ca^{2+} dynamics. Biophys J 84(1):28–41. https://doi.org/10.1016/s0006-3495(03)74830-9

Foehring RC, Zhang XF, Lee JCF, Callaway JC (2009) Endogenous calcium buffering capacity of substantia nigral dopamine neurons. J Neurophysiol 102(4):2326–2333. https://doi.org/10.1152/jn.00038.2009

Gabso M, Neher E, Spira ME (1997) Low mobility of the Ca^{2+} buffers in axons of cultured aplysia neurons. Neuron 18(3):473–481. https://doi.org/10.1016/s0896-6273(00)81247-7

Gilabert JA (2001) Energized mitochondria increase the dynamic range over which inositol 1,4,5-trisphosphate activates store-operated calcium influx. EMBO J 20(11):2672–2679. https://doi.org/10.1093/emboj/20.11.2672

Han JM, Periwal V (2019) A mathematical model of calcium dynamics: Obesity and mitochondria-associated ER membranes. Sneyd J, editor. PLOS Computational Biology. 15(8):e1006661.https://doi.org/10.1371/journal.pcbi.1006661

Jagtap Y, Adlakha N (2023) Numerical model of hepatic glycogen phosphorylase regulation by nonlinear interdependent dynamics of calcium and IP_3. Eur Phys J plus 138:399. https://doi.org/10.1140/epjp/s13360-023-03961-y

Jagtap Y, Adlakha N (2018) Finite volume simulation of two dimensional calcium dynamics in a hepatocyte cell involving buffers and fluxes. Commun Math Biol Neurosci 2018:15

Jagtap Y, Adlakha N (2019) Numerical study of one-dimensional buffered advection-diffusion of calcium and IP_3 in a hepatocyte cell. Netw Model Anal Health Inf Bioinformatics 8(1). https://doi.org/10.1007/s13721-019-0205-5

Jha A, Adlakha N (2014) Finite element model to study the effect of exogenous buffer on calcium dynamics in dendritic spines. Int J Model, Simul, Sci Comput 05(02):1350027. https://doi.org/10.1142/s179396231350027x

Jha A, Adlakha N, Jha BK (2016) Finite element model to study effect of Na +-C^{a2}+ exchangers and source geometry on calcium dynamics in a neuron cell. J Mech Med Biol 16(02):1650018. https://doi.org/10.1142/s0219519416500184

Jha A, Adlakha N (2015) Two-dimensional finite element model to study unsteady state Ca^{2+} diffusion in neuron involving ER LEAK and SERCA. Int J Biomath 08(01):1550002. https://doi.org/10.1142/s1793524515500023

Kumar H, Naik PA, Pardasani KR (2017) Finite Element Model to Study Calcium Distribution in T Lymphocyte Involving Buffers and Ryanodine Receptors. Proc Natl Acad Sci, India, Sect A 88(4):585-590.https://doi.org/10.1007/s40010-017-0380-7

Kopelman PG (2000) Obesity as a medical problem. Nature 404(6778):635–643

Kotwani M, Adlakha N (2017) Modeling of endoplasmic reticulum and plasma membrane Ca^{2+} uptake and release fluxes with excess buffer approximation (EBA) in fibroblast cell. Int J Comput Mater Sci Eng 06(01):1750004. https://doi.org/10.1142/s204768411750004x

Kotwani M, Adlakha N, Mehta MN (2014a) Finite element model to study the effect of buffers, source amplitude and source geometry on spatio-temporal calcium distribution in fibroblast cell. J Med Imaging Health Informatics 4(6):840–847. https://doi.org/10.1166/jmihi.2014.1328

Kotwani M, Adlakha N, Mehta MN (2014b) Intracellular calcium dynamics in fibroblast cell: A numerical study with two dimensional mathematical models. J Coupled Syst Multiscale Dynamics 2(4):238–243. https://doi.org/10.1166/jcsmd.2014.1058

Kothiya A, Adlakha N (2022) Model of calcium dynamics regulating IP_3 and ATP production in a fibroblast cell. Adv Syst Sci Appl 22(3):49–69

Kothiya AB, Adlakha N (2023) Cellular nitric oxide synthesis is affected by disorders in the interdependent Ca^{2+} and IP_3 dynamics during cystic fibrosis disease. J Biol Phys 49(2):133–158. https://doi.org/10.1007/s10867-022-09624-w

Klingauf J, Neher E (1997) Modeling buffered Ca^{2+} diffusion near the membrane. Biophys J 72(2):674–690. https://doi.org/10.1016/s0006-3495(97)78704-6

Lopez-Caamal F, Oyarzun DA, Middleton RH, Garcia MR (2014) Spatial quantification of cytosolic Ca^{2+} accumulation in nonexcitable cells: an analytical study. IEEE/ACM Trans Comput Biol Bioinf 11(3):592–603. https://doi.org/10.1109/tcbb.2014.2316010

Manhas N, Anbazhagan N (2021) A mathematical model of intricate calcium dynamics and modulation of calcium signalling by mitochondria in pancreatic acinar cells. Chaos, Solitons Fractals 145:110741. https://doi.org/10.1016/j.chaos.2021.110741

Manhas N, Pardasani KR (2014a) mathematical model to study IP_3 dynamics dependent calcium oscillations in pancreatic acinar cells. J Med Imaging Health Informatics 4(6):874–880. https://doi.org/10.1166/jmihi.2014.1333

Manhas N, Pardasani KR (2014b) Modelling mechanism of calcium oscillations in pancreatic acinar cells. J Bioenerg Biomembr 46(5):403–420. https://doi.org/10.1007/s10863-014-9561-0

Montalto D (2021) Focus on obesity. OBG Management 33(5). https://doi.org/10.12788/obgm.0095

Naraghi M, Neher E (1997) Linearized buffered ca2+ diffusion in microdomains and its implications for calculation of [Ca2+] at the mouth of a calcium channel. J Neurosci 17(18):6961–6973. https://doi.org/10.1523/jneurosci.17-18-06961.1997

Naik PA, Pardasani KR (2015) One dimensional finite element model to study calcium distribution in oocytes in presence of VGCC, RyR and buffers. J Med Imaging Health Informatics 5(3):471–476. https://doi.org/10.1166/jmihi.2015.1431

Neher E, Augustine GJ (1992) Calcium gradients and buffers in bovine chromaffin cells. J Physiol 450(1):273–301. https://doi.org/10.1113/jphysiol.1992.sp019127

Nowycky MC, Pinter MJ (1993) Time courses of calcium and calcium-bound buffers following calcium influx in a model cell. Biophys J 64(1):77–91. https://doi.org/10.1016/s0006-3495(93)81342-0

Patil J, Vaze A, Sharma L, Bachhav, A (2022). An Unsteady State case: calcium profiling based on temperature variation in neuronal cell due to Cancer Cells. In 2022 6th International Conference On Computing, Communication, Control And Automation ICCUBEA, IEEE, pp 1–6

Pawar A, Raj Pardasani K (2022) Effects of disorders in interdependent calcium and IP_3 dynamics on nitric oxide production in a neuron cell. Eur Phys J Plus 137(5). https://doi.org/10.1140/epjp/s13360-022-02743-2

Pawar A, Pardasani KR (2022a) Effect of disturbances in neuronal calcium and IP3 dynamics on β-amyloid production and degradation. Cogn Neurodyn 17(1):239–256. https://doi.org/10.1007/s11571-022-09815-0

Pawar A, Pardasani KR (2022b) Simulation of disturbances in interdependent calcium and -amyloid dynamics in the nerve cell. Eur Phys J Plus 137(8). https://doi.org/10.1140/epjp/s13360-022-03164-x

Pawar A, Pardasani KR (2022c) Study of disorders in regulatory spatiotemporal neurodynamics of calcium and nitric oxide. Cogn Neurodyn. https://doi.org/10.1007/s11571-022-09902-2

Pawar A, Pardasani KR (2023) Computational model of calcium dynamics-dependent dopamine regulation and dysregulation in a dopaminergic neuron cell. Eur Phys J Plus 138(1). https://doi.org/10.1140/epjp/s13360-023-03691-1

Pathak KB, Adlakha N (2015) Finite element model to study calcium signalling in cardiac myocytes involving pump, leak and excess buffer. J Med Imaging Health Informatics 5(4):683–688. https://doi.org/10.1166/jmihi.2015.1443

Panday S, Pardasani KR (2013) Finite element model to study effect of advection diffusion and Na +/C^{a2}+ Exchanger on C^{a2}+ distribution in oocytes. J Med Imaging Health Informatics 3(3):374–379. https://doi.org/10.1166/jmihi.2013.1184

Pi-Sunyer FX (2002) The medical risks of obesity. Obes Surg 12(S1):S6–S11. https://doi.org/10.1007/bf03342140

Prins D, Michalak M (2011) Organellar calcium buffers. Cold Spring Harb Perspect Biol 3(3):a004069–a004069. https://doi.org/10.1101/cshperspect.a004069

Schwaller B (2019) Cytosolic Ca^{2+} buffers are inherently Ca^{2+} signal modulators. Cold Spring Harbor Perspect Biol 12(1):a035543. https://doi.org/10.1101/cshperspect.a035543

Siso-Nadal F, Fox JJ, Laporte SA, Hébert TE, Swain PS (2009) Cross-Talk between Signaling Pathways Can Generate Robust Oscillations in Calcium and cAMP. Di Bernardo D, editor. PLoS One 4(10):e7189. https://doi.org/10.1371/journal.pone.0007189

Singh N, Adlakha N (2019) Nonlinear dynamic modeling of 2-dimensional interdependent calcium and inositol 1,4,5-trisphosphate in cardiac myocyte. Math Biol Bioinformatics 14(1):290–305. https://doi.org/10.17537/2019.14.290

Stern MD (1992) Buffering of calcium in the vicinity of a channel pore. Cell Calcium 13(3):183–192. https://doi.org/10.1016/0143-4160(92)90046-u

Smith GD (1996) Analytical steady-state solution to the rapid buffering approximation near an open Ca^{2+} channel. Biophys J 71(6):3064–3072. https://doi.org/10.1016/s0006-3495(96)79500-0

Smith GD, Wagner J, Keizer J (1996) Validity of the rapid buffering approximation near a point source of calcium ions. Biophys J 70(6):2527–2539. https://doi.org/10.1016/s0006-3495(96)79824-7

Singh N, Adlakha N (2019b) A mathematical model for interdependent calcium and inositol 1,4,5-trisphosphate in cardiac myocyte. Netw Model Anal Health Informatics Bioinformatics 8(1). https://doi.org/10.1007/s13721-019-0198-0

Singh N, Adlakha N (2019c) Three dimensional coupled reaction-diffusion modeling of calcium and inositol 1,4,5-trisphosphate dynamics in cardiomyocytes. RSC Adv 9(72):42459–42469. https://doi.org/10.1039/c9ra06929a

Tewari SG, Pardasani KR (2012) Modeling effect of sodium pump on calcium oscillations in neuron cells. J Multiscale Model 04(03):1250010. https://doi.org/10.1142/s1756973712500102

Tewari SG (2012) The sodium pump controls the frequency of action-potential-induced calcium oscillations. Comput Appl Math 31(2):283–304. https://doi.org/10.1590/s1807-03022012000200004

Vaishali, Adlakha N (2023) Disturbances in system dynamics of Ca^{2+} and IP_3 perturbing insulin secretion in a pancreatic β-cell due to type-2 diabetes. J Bioenergetics Biomembranes 1–17

Wacquier B, Combettes L, Van Nhieu GT, Dupont G (2016) Interplay between intracellular Ca^{2+} Oscillations and Ca^{2+}-stimulated mitochondrial metabolism. Sci Rep 6(1)19316. https://doi.org/10.1038/srep19316

Wagner J, Fall CP, Hong F, Sims CE, Allbritton NL, Fontanilla RA, Moraru II, Loew LM, Nuccitelli R (2004) A wave of IP_3 production accompanies the fertilization Ca^{2+} wave in the egg of the frog, Xenopus laevis: theoretical and experimental support. Cell Calcium 35(5):433–447. https://doi.org/10.1016/j.ceca.2003.10.009

Yripathi A, Adlakha N (2013) Finite element model to study calcium diffusion in a neuron cell involving JRYR, JSERCA and JLEAK. J Appl Math Informatics 31(5_6):695–709. https://doi.org/10.14317/jami.2013.695